Does the Rashba splitting in CH 3 NH 3 PbBr 3 arise from 2x2 surface reconstruction?

Xiaoyang Che, Boubacar Traoré, Claudine Katan, Mikael Kepenekian, Jacky Even

▶ **To cite this version:**

HAL Id: hal-01727137
https://hal.science/hal-01727137

Submitted on 15 Feb 2021

Does Rashba splitting in CH₃NH₃PbBr₃ arise from 2 × 2 surface reconstruction?†

Xiaoyang Che,[ab] Boubacar Traore, [ID][a] Claudine Katan, [ID][a] Mikaël Kepenekian [ID] *[a] and Jacky Even [ID] *[b]

As a result of early theoretical predictions, evidence for the Rashba or Dresselhaus effect in hybrid perovskites has recently attracted several experimental investigations, motivated by possible applications in spin-orbitronics. For instance, a large Rashba splitting has recently been reported for the (001) surface of CH₃NH₃PbBr₃. This effect is forbidden in the bulk material since both low-temperature and room-temperature crystal structures present inversion symmetry. Here we investigate the effects of two (001) nanoscale surface reconstructions of CH₃NH₃PbBr₃ using first-principles approaches based on density functional theory (DFT). The two experimental reconstructions are related to different orientations of MA cations at the surface, defining zigzag and dimer phases. The impact of these structural transformations on their electronic structures is thoroughly investigated. Whereas calculations reveal the occurrence of surface-induced Rashba effect, its amplitude is considerably smaller than the experimentally reported value, in agreement with other experimental investigations and leading to the conclusion that mesoscale surface polar domains and/or surface defects may result from sample preparation.

1 Introduction

Solution-processed halide perovskites have recently led to solar cells with outstanding power conversion efficiencies and low costs of production. Their highest record of light to electricity conversion efficiency has witnessed a spectacular increase from 3.8% in the pioneering work of Miyasaka and co-workers[1] in 2009 to 22.7% (NREL certificated) in 2017,[2,3] surpassing that of state-of-the-art thin film silicon based solar cells.[4,5] Very recently, fully inorganic perovskite quantum dots (CsPbI₃) also led to the record efficiency of the quantum dot cell technology.[2,6] More, their bulk and colloidal nanostructures present attractive photo- and electroluminescence properties with unusual giant relativistic effects in their band structures, which opened new paths in the field of optoelectronics.[7–10] However, fundamental studies remain essential in order to shed more light on the microscopic mechanisms at the origin of their exceptional optoelectronic properties.

One main feature of halide perovskites is the presence of heavy atoms such as lead, tin or iodine that leads to a strong spin–orbit coupling (SOC) effect.[11–14] Combining this effect

with the loss of inversion symmetry gives rise to strong spinor splitting of Rashba, Dresselhaus or mixed Rashba–Dresselhaus types[15–17] in both or either the conduction and valence bands.[13,18–22] Such an effect would open the way to halide perovskite-based spintronics and spin-orbitronics.[23,24] Direct evidence for the Rashba effect in hybrid perovskites was recently inspected using angle-resolved photoemission spectroscopy (ARPES) on CH₃NH₃PbBr₃ (MA = CH₃NH₃⁺) single crystals, which delivered contradictory outcomes.[25,26] Both experiments were performed on the (001) surfaces of MAPbBr₃. Whereas Komesu *et al.*[25] did not evidence any effect related to k-dependent spin-splitting in their room temperature experiments, Niesner *et al.*,[26] after great care in sample surface preparation, reported giant splittings of 7 ± 1 eV Å and 11 ± 4 eV Å for low temperature orthorhombic and high temperature cubic phases, respectively. To the best of our knowledge, these values correspond to the largest Rashba effects ever recorded by ARPES. Meanwhile, specific patterns of the orientations of MA have been observed on the (001) surface of MAPbBr₃ by scanning tunneling microscopy (STM), resulting in local ferroelectric and antiferroelectric domains, which could enhance surface spin-splitting.[27] So far, no theoretical approach has addressed the impact of nanoscale surface reconstructions on spinor splitting phenomena and such work would benefit the microscopic understanding of hybrid perovskites.

Here, within the framework of density functional theory (DFT),[28,29] we first describe the experimental surface reconstructions of the (001) oriented facets of MAPbBr₃ in its orthorhombic phase. The collective orientations of MA cations

[a] *Univ Rennes, ENSCR, INSA Rennes, CNRS, ISCR – UMR 6226, F-35000 Rennes, France. E-mail: mikael.kepenekian@univ-rennes1.fr*
[b] *Univ Rennes, INSA Rennes, CNRS, Institut FOTON – UMR 6082, F-35000 Rennes, France. E-mail: jacky.even@insa-rennes.fr*

give rise to two phases, which are referred to as dimer and zigzag phases, consistently with STM topography images.[27] Then, the impact of reconstructions on the electronic properties is inspected. The resulting band splitting computed at the (001) surface is found to be much weaker than the measured one reported by Niesner et al.[26] Thus, it is unlikely that such a nanoscale reconstruction by itself is at the origin of the strong Rashba splitting observed in these ARPES experiments.

2 Method

2.1 Computational details

DFT calculations are performed using the SIESTA simulation package.[30] Structure relaxations are carried out using the C09 functional that takes into account van der Waals interactions.[31] All self-consistent calculations are performed including SOC. To prevent conflicts between the on-site treatment of SOC within SIESTA and the non-locality of C09, single-point calculations are conducted using the revPBE functional on which C09 is based. Core electrons are described using norm-conserving Troullier–Martins pseudopotentials.[32] $1s^1$, $2s^2 2p^2$, $2s^2 2p^3$, $4s^2 4p^5$, and $5d^{10} 6s^2 6p^2$ are used as valence electrons for H, C, N, Br and Pb respectively. The valence wavefunctions are expanded over a double-ζ polarized basis set of finite-range numerical pseudoatomic orbitals.[33] An energy cutoff of 150 Ry for the real-space mesh is used. Structure optimisations are considered to be converged when the maximum residual force on each atom becomes smaller than 0.04 eV Å^{-1}. The Brillouin-zones (BZ) are sampled with $4 \times 4 \times 4$ and $3 \times 3 \times 1$ Monkhorst–Pack k-grids for bulk systems and slabs, respectively. The dipoles induced in the slabs are treated with the dipole correction scheme[34] as implemented in SIESTA.

2.2 Construction of the (001) surface of MAPbBr$_3$

First we design and build the relevant (001) surface. We start from the orthorhombic *Pnma* low temperature crystallographic structure of MAPbBr$_3$.[35] To preserve a similar crystallographic orientation to the one used in the ARPES experiments,[26,27] we use the Pbnm setting, which is deduced from *Pnma* by a rotation of the coordinate system where the lattice parameters read $a = 8.59$ Å, $b = 7.94$ Å, $c = 11.85$ Å. Then, relaxing both the lattice parameters and atomic positions of bulk MAPbBr$_3$ leads to the following lattice parameters: $a = 8.71$ Å, $b = 7.70$ Å and $c = 11.80$ Å (Fig. 1a), corresponding to a 3% expansion along the a-axis, 1.4% and 0.4% contractions along the b and c-axes, respectively. We checked that relaxation does not alter the orientation of the 4 nearest neighbor organic molecules, maintaining a similar ordering to that in the experimental bulk structure related to an antiferroelectric configuration.[35] Regarding surface termination, there is experimental evidence for MA–halogen termination (Fig. S1, ESI†) for the (001) surface of both cubic MAPbBr$_3$[25] and orthorhombic MAPbI$_3$.[36] Thus, we focus on the (001) surface of MAPbBr$_3$ terminated by MA–Br (Fig. 1b). Starting from the bulk unit cell of MAPbBr$_3$, we first double its size in the (a,b) plane perpendicular to the surface
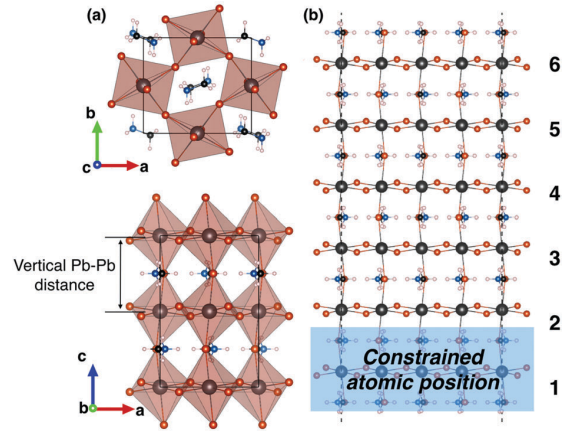

Fig. 1 Bulk and surface structures of MAPbBr$_3$. (a) View along (001) and (010) of the bulk structure of the orthorhombic MAPbBr$_3$ in the *Pnma* space group. (b) Slab of MAPbBr$_3$ having a (001) surface, terminated by Br atoms and MA cations, used to inspect surface reconstruction. Layers are labelled 1–6 from the bulk to the surface.

and then add a vacuum region of 85 Å along the c-axis in order to minimize periodic electrostatic interactions. The resulting MAPbBr$_3$ slab contains six PbBr$_6$ octahedra along the c-axis. During structure optimization, the lattice parameters are fixed and the bottom octahedron (layer 1 in Fig. 1b) is kept frozen in the bulk configuration, while the rest of the structure is allowed to relax.

3 Results and discussion

3.1 (001) surface reconstructions

The relaxation of the atomic positions at the (001) surface leads to two different reconstructions namely the zigzag and dimer phases (Fig. 2a and b). In the so-called zigzag phase, MA cations are organized in a way similar to the bulk structure, *i.e.* the organic molecules are oriented in a non-parallel manner. On the other hand, the dimer phase is obtained as a result of the in-plane rotation of half of MA cations on the top layer (layer 6) followed by the full optimization of atomic positions leading to a parallel configuration of MA cations corresponding to a rotation angle of $\sim 26°$. The dimer phase is 350 meV per supercell higher in energy than the zigzag phase, which amounts to 7.3 meV per MAPbBr$_3$ unit. This value compares well with the energetic cost corresponding to the rotation of MA cations in MAPbI$_3$.[37] The zigzag phase would therefore be the dominant one, however, the energy difference does not preclude the coexistence of both phases, as observed experimentally.[27] As expected, the in-plane Pb–Br bonds show no significant sign of elongation or contraction, as compared to those of the frozen layer 1 in the bulk configuration (Table S1, ESI†). The same is observed for the out-of-plane Pb–Br bonds and the vertical Pb–Pb distances, except for the top layer that undergoes elongations of 0.05 Å and ~ 0.10 Å, respectively, indicative of sizable surface breathing. Thus, the PbBr$_6$ unit preserves its quasi-octahedral geometry except for the top layer that shows stretching in the (001) direction.
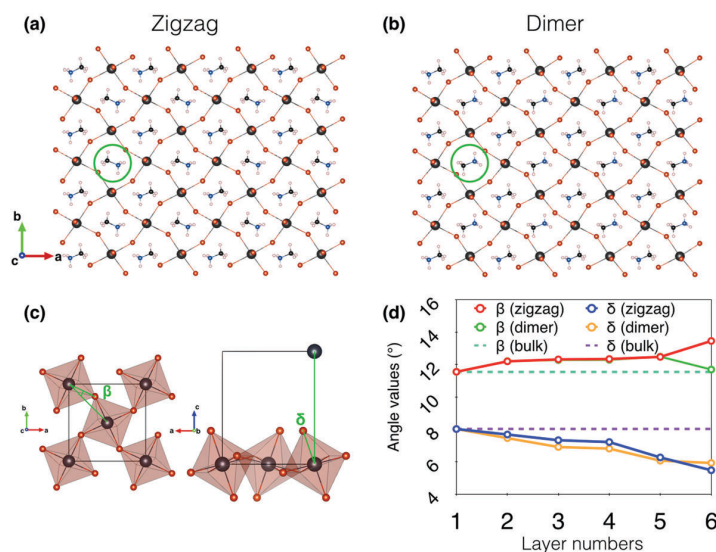
Fig. 2 (001) surface reconstructions of MAPbBr$_3$ characterized by the rotation of MA cations. (a) (001) surface in the zigzag phase. (b) Same for the dimer phase. (c) Definition of the in-plane, β, and out-of-plane, δ, octahedron tilt angles. (d) Variation of the average tilt angles β and δ from the bulk (layer 1) to the surface (layer 6, Table S1, ESI†).

Moreover, the corner-shared structure of halide perovskites provides additional degrees of freedom, namely for distortions which can be quantified by two characteristic angles: the in-plane (β) and out-of-plane (δ) octahedron tilts (Fig. 2c).[38] Fig. 2d shows the evolution of β and δ on going from the bulk to the surface. Unlike the bond lengths where little variations are observed between the bulk and surface layers, the octahedron tilt angles undergo significant changes. For both the zigzag and dimer phases, δ decreases progressively from the bulk to the surface (Table S1, ESI†). Noteworthily, surface octahedra show the lowest δ tilt angles and are similar in the zigzag and dimer phases. This is not the case for the in-plane tilting β. In particular, β of the top layer remains close to the bulk value in the dimer phase, whereas β increases from $\sim 11.5°$ in the bulk to $\sim 13.5°$ on the surface of the zigzag phase. A direct consequence of this contrast is that Br–Br distances largely differ between the two phases (Fig. 3). Indeed, in the case of the zigzag case, all Br–Br distances at the surface maintain the same trend as in the relaxed bulk, although the values are

enlarged due to the surface effect. Meanwhile, because of the MA rotations, the dimer phase shows an alternation between short (~ 5.14 Å) and large (~ 6.49 Å) distances (Fig. 3b and c). This distinctive behaviour between the zigzag and dimer phases is at the origin of the striking differences observed in the recorded STM images.[27]

3.2 Electronic structure

Bulk MAPbBr$_3$ retains the major features of the well-known MAPbI$_3$ halide perovskite. Typically, the electronic band structure of the orthorhombic phase presents a direct band gap at Γ with a DFT energy band gap (including SOC) of about 1.1 eV.[14] The highest valence states mainly arise from Br(4p) and Pb(6s) orbitals with anti-bonding hybridization, whereas the lowest conduction bands mainly originate from Pb(6p) orbitals (Fig. S3, ESI†). When moving from the bulk to the surface, the gap seemingly remains direct at Γ for both the zigzag and dimer phases (Fig. 4a and b, respectively). As a result of performing slab calculations to emulate the (001) surface and
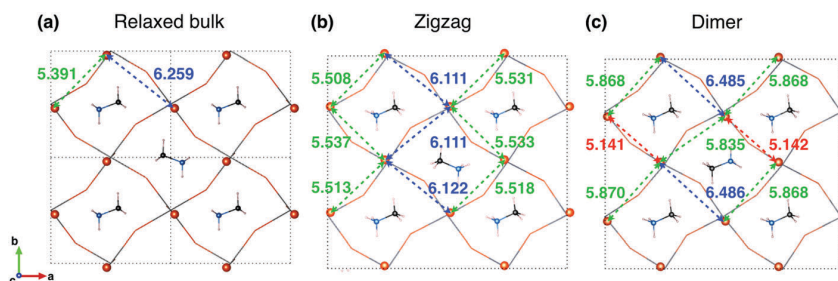

Fig. 3 Bond-lengths of inequivalent Br–Br distances (Å) at the surface for (a) the bulk, (b) the zigzag phase, and (c) the dimer phase. Dotted lines indicate the limit of the unit cell.
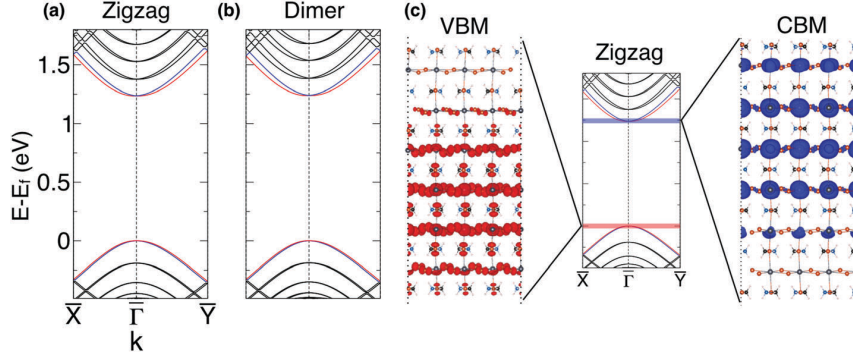
Fig. 4 Electronic properties of the reconstructed surfaces. Electronic band structures including SOC for the relaxed (a) zigzag and (b) dimer phases. The direct band gap amounts to 1.2 eV for both phases. (c) LDOS of the VBM and the CBM for the relaxed zigzag phase (see Fig. S4, ESI† for the dimer phase).

despite the 6-octahedron thickness of the slab, the system still experiences quantum confinement leading to a band gap opening that now amounts to 1.2 eV. Noteworthily, this is consistent with the experimental band structure obtained by ARPES.[25]

A direct consequence of surface relaxation is the localization of valence and conduction band densities.[39] In order to illustrate this point, we calculate the local density of states (LDOS) at the valence band maximum (VBM) and the conduction band minimum (CBM) for the zigzag (Fig. 4c) and dimer phases (Fig. S3, ESI†). The main features of the bulk are preserved: VBMs exhibit contributions from Br(4p) and Pb(6s) orbitals, and CBMs from Pb(6p) ones. However, in the relaxed structures, the contribution of the VBM decreases at the surface and shifts toward the inner bulk layers, while the CBM gains significant weight on the surface. Importantly, this leads to the creation of a surface dipole reaching -7.2 Debye for the zigzag phase and -6.6 Debye for the dimer phase (the dipole is vanishing prior to surface relaxation). Interestingly, no remarkable difference between the LDOS of the zigzag and dimer phases can be noticed. Thus, the specific configuration of the MA molecules on the top of the surface is found to have little influence on neither charge densities at the band edges, band dispersions nor band gaps.

3.3 Rashba effect

A closer look at the band structures reveals that the VBMs (resp. CBMs) are split when SOC is included resulting in a shift of maxima (resp. minima) of energy away from Γ (Fig. 5a and b). Such a splitting is characteristic of the Rashba–Desselhaus effect.[15,17] The latter is a consequence of the combined effect of a giant SOC and the loss of inversion symmetry caused by surface structural relaxation. It has been first described in zinc-blende semiconductors and wurtzite structures and later generalized to quasi-2-dimensional systems.[15–17] Since it has been characterized in semiconductor heterostructures,[40] bulks with layered structures[41] or heavy atom surfaces.[42] Its amplitude is quantified by a parameter α defined as $\alpha = 2E_0/k_0$, where E_0 is the splitting energy and k_0 the momentum shift of the maximum or the minimum of energy away from the high symmetry point (Fig. 5b). The calculated Rashba parameters α
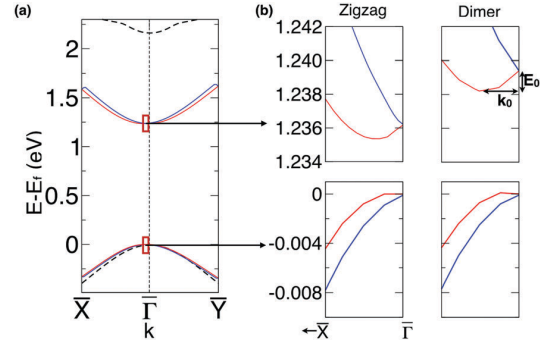

Fig. 5 Rashba effect in the reconstructed surfaces. (a) Electronic band structure of the zigzag phase with (straight lines) and without (dashed lines) SOC. (b) Zoom in the dispersions of the VBM and the CBM revealing the Rashba spinor splitting for each of the two reconstructed phases. Definition of E_0 and k_0, respectively, the energy splitting and momentum shift, needed to define the Rashba parameter $\alpha = 2E_0/k_0$ is also shown.

for the zigzag and dimer phases are computed to be 0.59 eV Å (0.24 eV Å) and 0.44 eV Å (0.27 eV Å) for the CBM (VBM), respectively (Table 1). These calculated values are more than one order of magnitude smaller than the values (7 ± 1 eV Å for the VBM) extracted from ARPES experiments performed over cleaved single crystals of MAPbBr$_3$.[26] Moreover, given the small difference computed between the zigzag and dimer phases, one can hardly explain these experimental values on the basis of simple surface reconstructions associated with the flip of half of surface MA molecules. Among possible interpretations, it

Table 1 The Rashba parameter α for both phases are calculated using the following expression: $\alpha = 2E_0/k_0$. E_0 represents the splitting energy and k_0 the momentum shift of the maximum or the minimum of energy away from the high symmetry point

Slabs		E_0 (10^{-4}) (eV)	k_0 (Å)	α (eV Å)
Zigzag	CBM	8.00	0.0027	0.59
	VBM	1.32	0.0011	0.24
Dimer	CBM	12.00	0.0055	0.44
	VBM	2.84	0.0021	0.27

could be associated with larger polar surface reconstructions and the creation of mesoscale ferroelectric domains.[43] Indeed, the beams used in ARPES cover surface areas that are much larger than the ones considered in the present DFT study. Unfortunately, such large supercell simulations are beyond available computational resources. Alternatively, despite the careful use of freshly cleaved surfaces,[26,44] the discrepancy of the results could originate from the presence of defects at the crystal surface in the experimental setup. As Rashba splitting is very sensitive to the local symmetry, the presence of defects could lead to large values of α escaping our description of a flawless surface. Other fascinating experimental results have been reported for surface-dependent optoelectronic properties of the halide perovskites and especially MAPbBr$_3$. There is indeed a strong interplay between ultravacuum conditions and the chemistry of the surface.[45] Moreover, our findings of noticeably smaller Rashba splitting is also supported by the second set of ARPES experiments performed over single crystals of MAPbBr$_3$ by another group,[25] which makes no mention of Rashba splitting, indicating that if any it is below their experimental resolution.

4 Conclusion

In summary, we investigated the (001) surface of the low-temperature orthorhombic phase of MAPbBr$_3$ and the effect of surface relaxation on the electronic properties. In agreement with recent STM experiments, we inspected two 2 × 2 (001) nanoscale surface reconstructions considering zigzag and dimer phases, which are characterized by different orientations of MA cations at the surface. First, for both phases surface reconstruction leads to sizeable elongation of the surface Pb–Pb bond lengths whereas the bottom layers remain similar to the bulk structure. Concomitantly, the surface in-plane octahedron tilt angles increase whereas the out-of-plane tilt angles decrease. Except for a slight increase of the band gap as a result of quantum confinement related to the finite and limited thickness of the slabs, the overall band structure remains similar to that computed for the bulk. Interestingly, the valence and conduction band densities reveal different spatial localizations, with the former pushing towards the bulk whereas the later gaining significantly more weight on the surface octahedra. Besides, a detailed inspection of the valence and conduction band dispersions of the reconstructed surface reveals the existence of the Rashba effect, both in valence and conduction bands, as a result of inversion symmetry breaking in the presence of strong spin–orbit coupling. However, the computed spinor splittings are more than an order of magnitude smaller than those experimentally reported for MAPbBr$_3$,[26] indicating that these experimental observations cannot be traced back to the atomic scale 2 × 2 surface reconstruction considered in our study. Thus such huge Rashba parameters are either related to mesoscale polar reconstructions, which do no correspond to the local ones evidenced by STM,[27] or to the presence of defects at the surface of the MAPbBr$_3$ single crystal.

The examination of punctual defects, *e.g.* vacancies, as well as step-edges will be carried out in the future.

Conflicts of interest

There are no conflicts to declare.

Acknowledgements

References

1 A. Kojima, K. Teshima, Y. Shirai and T. Miyasaka, *J. Am. Chem. Soc.*, 2009, **131**, 6050–6051.

2 NREL chart, https://www.nrel.gov/pv/assets/images/efficiency-chart.png.

3 W. S. Yang, B.-W. Park, E. H. Jung, N. J. Jeon, Y. C. Kim, D. U. Lee, S. S. Shin, J. Seo, E. K. Kim, J. H. Noh and S. I. Seok, *Science*, 2017, **356**, 1376–1379.

4 M. A. Green, *Prog. Photovoltaics Res. Appl.*, 2011, **20**, 472.

5 K.-H. Lee, K. Araki, L. Wang, N. Kojima, Y. Ohshita and M. Yamaguchi, *Prog. Photovoltaics Res. Appl.*, 2016, **24**, 1310.

6 E. M. Sanehira, A. R. Marshall, J. A. Christians, S. P. Harvey, P. N. Ciesielski, L. M. Wheeler, P. Schulz, L. Y. Lin, M. C. Beard and J. M. Luther, *Sci. Adv.*, 2017, **3**, eaao4204.

7 C. C. Stoumpos, C. D. Maliakas and M. G. Kanatzidis, *Inorg. Chem.*, 2013, **52**, 2013.

8 K. Tvingstedt, O. Malinkiewicz, A. Baumann, C. Deibel, H. J. Snaith, V. Dyakonov and H. J. Bolink, *Sci. Rep.*, 2014, **4**, 6071.

9 Y. Yamada, T. Nakamura, M. Endo, A. Wakamiya and Y. Kanemitsu, *IEEE J. Photovolt.*, 2015, **5**, 401.

10 H. Huang, L. Polavarapu, J. A. Sichert, A. S. Susha, A. S. Urban and A. L. Rogach, *NPG Asia Mater.*, 2016, **8**, e328.

11 J. Even, L. Pedesseau, M.-A. Dupertuis, J.-M. Jancu and C. Katan, *Phys. Rev. B: Condens. Matter Mater. Phys.*, 2012, **86**, 205301.

12 J. Even, L. Pedesseau, J.-M. Jancu and C. Katan, *J. Phys. Chem. Lett.*, 2013, **4**, 2999.

13 J. Even, L. Pedesseau, J.-M. Jancu and C. Katan, *Phys. Status Solidi RRL*, 2014, **8**, 31–35.

14 C. Katan, L. Pedesseau, M. Kepenekian, A. Rolland and J. Even, *J. Mater. Chem. A*, 2015, **3**, 9232–9240.

15 G. Dresselhaus, *Phys. Rev.*, 1955, **100**, 580.

16 Y. A. Bychkov and E. I. Rashba, *J. Exp. Theor. Phys.*, 1984, **39**, 78.

17 E. I. Rashba, *Phys. Solid State*, 1960, **2**, 1224.

18 M. Kim, J. Im, A. J. Freeman, J. Ihm and H. Jin, *Proc. Natl. Acad. Sci. U. S. A.*, 2014, **111**, 6900.

19 F. Brivio, K. T. Butler and A. Walsh, *Phys. Rev. B: Condens. Matter Mater. Phys.*, 2014, **89**, 155204.

20 A. Amat, E. Mosconi, E. Ronca, E. Quarti, P. Umari, M. K. Nazeeruddin, M. Grätzel and F. D. Angelis, *Nano Lett.*, 2014, **14**, 3608–3616.

21 A. Stroppa, D. Di Sante, P. Barone, M. Bokdam, G. Kresse, C. Franchini, M. H. Whangbo and S. Picozzi, *Nat. Commun.*, 2014, **5**, 5900.

22 M. Kepenekian, R. Robles, C. Katan, D. Sapori, L. Pedesseau and J. Even, *ACS Nano*, 2015, **9**, 11557.

23 E. Mosconi, T. Etienne and F. De Angelis, *J. Phys. Chem. Lett.*, 2017, **8**, 2247.

24 M. Kepenekian and J. Even, *J. Phys. Chem. Lett.*, 2017, **8**, 3362–3370.

25 T. Komesu, X. Huang, T. R. Paudel, Y. B. Losovyj, X. Zhang, E. F. Schwier, Y. Kojima, M. Zheng, H. Iwasawa, K. Shimada, M. I. Saidaminov, D. Shi, A. L. Abdelhady, O. M. Bakr, S. Dong, E. Y. Tsymbal and P. A. Dowben, *J. Phys. Chem. C*, 2016, **120**, 21710.

26 D. Niesner, M. Wilhelm, I. Levchuk, A. Osvet, S. Shrestha, M. Batentschuk, C. Brabec and T. Fauster, *Phys. Rev. Lett.*, 2016, **117**, 126401.

27 R. Ohmann, L. K. Ono, H.-S. Kim, H. Lin, M. V. Lee, Y. Li, N.-G. Park and Y. Qi, *J. Am. Chem. Soc.*, 2015, **137**, 16049.

28 P. Hohenberg and W. Kohn, *Phys. Rev.*, 1964, **136**, B864–B871.

29 W. Kohn and L. J. Sham, *Phys. Rev.*, 1965, **140**, A1133–A1138.

30 J. M. Soler, E. Artacho, J. D. Gale, A. García, J. Junquera, P. Ordejón and D. Sánchez-Portal, *J. Phys.: Condens. Matter*, 2002, **14**, 2745–2779.

31 V. R. Cooper, *Phys. Rev. B: Condens. Matter Mater. Phys.*, 2009, **81**, 161104.

32 N. Troullier and J. L. Martins, *Phys. Rev. B: Condens. Matter Mater. Phys.*, 1991, **43**, 1993.

33 D. Sánchez-Portal, E. Artacho, P. Ordejón, A. García and J. M. Soler, *Phys. Status Solidi*, 1999, **215**, 809.

34 L. Bengtsson, *Phys. Rev. B: Condens. Matter Mater. Phys.*, 1999, **59**, 12301–12304.

35 I. P. Swainson, R. Hammond, C. Soullière, O. Knop and W. Massa, *J. Solid State Chem.*, 2003, **176**, 97.

36 L. She, M. Liu and D. Zhong, *ACS Nano*, 2015, **10**, 1126–1131.

37 Y. Li, M. Behtash, J. Wong and K. Yang, *J. Phys. Chem. C*, 2018, **122**, 177–184.

38 L. Pedesseau, D. Sapori, B. Traore, R. Robles, H. H. Fang, M.-A. Loi, H. Tsai, W. Nie, J.-C. Blancon, A. J. Neukirch, S. Tretiak, A. D. Mohite, C. Katan, J. Even and M. Kepenekian, *ACS Nano*, 2016, **10**, 9776.

39 M. Kepenekian, B. Traore, J.-C. Blancon, L. Pedesseau, H. Tsai, W. Nie, C. C. Stoumpos, M. G. Kanatzidis, J. Even, A. D. Mohite, S. Tretiak and C. Katan, 2018, arXiv: 1801.00704.

40 J. Nitta, T. Akazaki, H. Takayanagi and T. Enoki, *Phys. Rev. Lett.*, 1997, **78**, 1335.

41 K. Ishizaka, M. Bahramy, H. Murakawa, M. Sakano, T. Shimojima, T. Sonobe, K. Koizumi, S. Shin, H. Miyahara, A. Kuimura, K. Miyamoto, T. Okuda, H. Namatame, M. Taniguchi, R. Arita, N. Nagaosa, K. Kobayashi, Y. Murakami, R. Kumai, Y. Kaneko, Y. Onose and Y. Tokura, *Nat. Mater.*, 2011, **10**, 521.

42 S. LaShell, B. A. McDougall and E. Jensen, *Phys. Rev. Lett.*, 1996, **77**, 3419.

43 Y. Kutes, L. Ye, Y. Zhou, S. Pang, B. D. Huey and N. P. Padture, *J. Phys. Chem. Lett.*, 2014, **5**, 3335.

44 D. Niesner, O. Schuster, M. Wilhelm, I. Levchuk, A. Osvet, S. Shrestha, M. Batentschuk, C. Brabec and T. Fauster, *Phys. Rev. B: Condens. Matter Mater. Phys.*, 2017, **95**, 075207.

45 H.-H. Fang, S. Adjokatse, H. Wei, J. Yang, G. R. Blake, J. Huang, J. Even and M.-A. Loi, *Sci. Adv.*, 2016, **2**, e1600534.

This journal is © the Owner Societies 2018

Phys. Chem. Chem. Phys., 2018, **20**, 9638–9643 | 9643